

Seven new binaries discovered in the *Kepler* light curves through the BEER method confirmed by radial-velocity observations

S. Faigler and T. Mazeh

School of Physics and Astronomy, Raymond and Beverly Sackler Faculty of Exact Sciences,
Tel Aviv University, Tel Aviv 69978, Israel

and

S. N. Quinn and D. W. Latham

Harvard-Smithsonian Center for Astrophysics, 60 Garden St., Cambridge, MA 02138

and

L. Tal-Or

School of Physics and Astronomy, Raymond and Beverly Sackler Faculty of Exact Sciences,
Tel Aviv University, Tel Aviv 69978, Israel

Received _____; accepted _____

ABSTRACT

We present seven newly discovered *non-eclipsing* short-period binary systems with low-mass companions, identified by the recently introduced BEER algorithm, applied to the publicly available 138-day photometric light curves obtained by the *Kepler* mission. The detection is based on the beaming effect (sometimes called Doppler boosting), which increases (decreases) the brightness of any light source approaching (receding from) the observer, enabling a prediction of the stellar Doppler radial-velocity modulation from its precise photometry. The BEER algorithm identifies the BEaming periodic modulation, with a combination of the well known Ellipsoidal and Reflection/heating periodic effects, induced by short-period companions. The seven detections were confirmed by spectroscopic radial-velocity follow-up observations, indicating minimum secondary masses in the range of 0.07–0.4 M_{\odot} . The discovered binaries establish for the first time the feasibility of the BEER algorithm as a new detection method for short-period non-eclipsing binaries, with the potential to detect in the near future non-transiting brown dwarfs secondaries, or even massive planets.

Subject headings: methods: data analysis — planetary systems: detection — binaries: spectroscopic — brown dwarfs

1. Introduction

In a recent paper Faigler & Mazeh (2011) presented a new way to discover short-period non-eclipsing binaries with low-mass companions by using highly precise photometric light curves obtained by space missions, like CoRoT and *Kepler* (Rouan et al. 1998; Baglin et al. 2006; Borucki et al. 2010). The algorithm, BEER, based on an idea suggested by Loeb & Gaudi (2003) and Zucker, Mazeh & Alexander (2007), searches for the beaming effect, sometimes called Doppler boosting, induced by stellar radial motion. This effect causes an increase (decrease) of the brightness of any light source approaching (receding from) the observer (Rybicki & Lightman 1979), on the order of $4v_r/c$, where v_r is the radial velocity of the source, and c is the velocity of light. Therefore, periodic modulation of the stellar velocity due to a companion in a binary orbit will produce a corresponding periodic beaming modulation of the stellar photometry.

For short-period binaries the beaming effect is extremely small, on the order of 100–300 ppm (parts per million). Therefore the effect has become relevant only recently, when CoRoT and *Kepler* — the two presently operating satellites that search for transiting exoplanets, started producing hundreds of thousands of uninterrupted light curves with high precision (Auvergne et al. 2009; Koch et al. 2010).

As predicted, several studies detected the beaming effect in eclipsing binaries and transiting planets, for which the orbital period was well established from the space-obtained light curves (van Kerkwijk et al. 2010; Rowe et al. 2010; Carter et al. 2010; Mazeh & Faigler 2010; Bloemen et al. 2011; Kipping & Spiegel 2011). Yet, space mission data can yield much more. Evidence of the binarity of a stellar system can be found from detecting the beaming effect without any eclipse or transit (Loeb & Gaudi 2003; Zucker, Mazeh & Alexander 2007). However, the beaming modulation by itself might not be enough to render a star a good binary candidate, as periodic modulations could be produced by other effects, stellar

variability in particular (Aigrain, Favata & Gilmore 2004).

The BEER detection algorithm (Faigler & Mazeh 2011), therefore, searches for stars that show in their light curves a combination of the BEaming effect with two other effects induced by the presumed companion — the Ellipsoidal and the Reflection modulation. The ellipsoidal variation (Morris 1985) is due to the tidal distortion of each component by the gravity of its companion (see a review by Mazeh (2008)), while the reflection/heating variation (referred to herein as the reflection modulation) is induced by the luminosity of each component that falls only on the close side of its companion (Vaz 1985; Wilson 1990; Maxted et al. 2002; Harrison et al. 2003; For et al. 2010; Reed et al. 2010). Detecting the beaming effect together with the ellipsoidal and reflection modulations, with the expected relative amplitudes and *phases* in particular, can suggest the presence of a small non-transiting companion.

Just as transit searches, the candidates found by the BEER algorithm have to be followed by radial-velocity (RV) observations, in order to confirm the existence of the low-mass companion, and to reject other possible interpretations of the photometric modulation.

This paper presents the discovery of the first seven new binaries with low-mass secondaries, in the range of $0.07\text{--}0.4 M_{\odot}$, detected by using the BEER algorithm, and confirmed by RV spectroscopic follow-up measurements. Section 2 presents the photometric analysis of the *Kepler* light curves, Section 3 provides the details and results of the RV observations, Section 4 summarizes and compares the results of the photometric analysis and the RV measurements, and Section 5 discusses the implications of, and conclusions from, the findings of this paper.

2. Photometric analysis

We used the publicly available *Kepler* raw light curves of the Q0, Q1 and Q2 quarters, spanning 138 days. To avoid systematic variations, we ignored all data points within 1 day after the beginning of Q2, and all data points within 1 day before, to 3 days after, each of the two safe mode events in Q2. We also corrected two systematic jumps at *Kepler* time ($JD - 2454833$) of 200.32 and 246.19 days. We then applied the BEER algorithm to 14,685 stars brighter than 13th mag, with *Kepler* Input Catalog (Brown et al. 2011) radius smaller than $3R_{\odot}$, calculating the BEER periodogram (Faigler & Mazeh 2011) with period range of 0.5–20 days for each star. Next, we identified the periodograms whose highest peak was at least 3 time higher than the next highest one. For these stars we used the peak period to estimate the system secondary mass and radius, assuming the periodicity is induced by a secondary star. We then selected 25 candidates with secondary mass smaller than $0.5M_{\odot}$ and implied albedo smaller than 0.4, suggesting a significant probability for a low-mass companion. These candidates were then followed by RV observations, which we describe in detail in the next section. In a forthcoming paper we will report on the false alarm cases, and analyze the false alarm frequency of our candidates. Here we report on the first seven clear detections.

Table 1 lists for each of the seven stars its coordinates, the stellar properties estimates from the Kepler Input Catalog (Brown et al. 2011), the photometric periods and amplitudes of the three effects found by the BEER algorithm, and the r.m.s. of the data before and after subtraction of the BEER model.

We order the stars according to the detected RV amplitude, presented in the next section. Figure 1 presents the ‘cleaned’ (Mazeh & Faigler 2010; Faigler & Mazeh 2011) photometric data of the seven detections, Figure 2 presents the BEER periodograms for the detections, and Figure 3 shows the light curves folded with the detected period. In fact, the

quality of the *Kepler* data is so high that the periodic modulation can be seen directly from the cleaned data, plotted in Figure 1, even without consulting the BEER periodogram.

It is interesting to compare the shape of the BEER modulation of the seven candidates, presented in Fig 3. In six of them the two peaks, at phase of 0.25 and 0.75, are similar, although the latter is somewhat smaller, due to the beaming effect (Faigler & Mazeh 2011). In one case, K08016222, the second peak completely disappeared, because in this case the beaming amplitude is more than three times higher than that of the ellipsoidal, while for the rest of the candidates, the ellipsoidal amplitude is significantly higher than the beaming amplitude. This is a clear result of the long orbital period and small stellar radius of this system, relative to the other systems, since the ellipsoidal amplitude to beaming amplitude ratio is proportional to $R_*^3/P_{orb}^{5/3}$ (Faigler & Mazeh 2011; Zucker, Mazeh & Alexander 2007).

Table 1. Coordinates, magnitudes, stellar properties, and photometric analysis results of the seven candidates

	K10848064	K08016222	K09512641	K07254760	K05263749	K04577324	K06370196
RA	19:01:21.24	19:06:48.03	18:58:39.91	18:42:28.78	19:12:59.00	19:42:35.91	19:35:00.36
DEC	48:16:32.90	43:48:32.90	46:08:52.80	42:49:31.90	40:26:42.30	39:38:00.80	41:47:59.60
K_p^a [mag]	12.13	11.65	11.66	12.04	11.53	11.98	11.97
R^a [R_\odot]	1.5	1.3	1.7	1.5	1.9	1.3	2.1
M^b [M_\odot]	1.2	1.1	1.2	1.2	1.3	1.2	1.3
Photometry results:							
Period [days]	3.49 ± 0.01	5.60 ± 0.02	4.65 ± 0.02	2.66 ± 0.01	3.73 ± 0.01	2.33 ± 0.01	4.23 ± 0.01
Ellipsoidal [ppm]	201 ± 3	30 ± 2	172 ± 10	845 ± 7	1222 ± 5	1489 ± 4	1210 ± 10
Beaming [ppm]	118 ± 3	97 ± 2	185 ± 5	356 ± 6	358 ± 5	436 ± 4	382 ± 7
Reflection [ppm]	0 ± 3	6 ± 2	36 ± 4	150 ± 6	158 ± 5	245 ± 4	174 ± 7
Cleaned data r.m.s. [ppm]	204	106	227	807	1184	1408	1141
Residuals r.m.s. [ppm]	128	68	113	268	200	168	328

^a from Kepler Input Catalog

^b calculated from Kepler Input Catalog $\log g$ and R

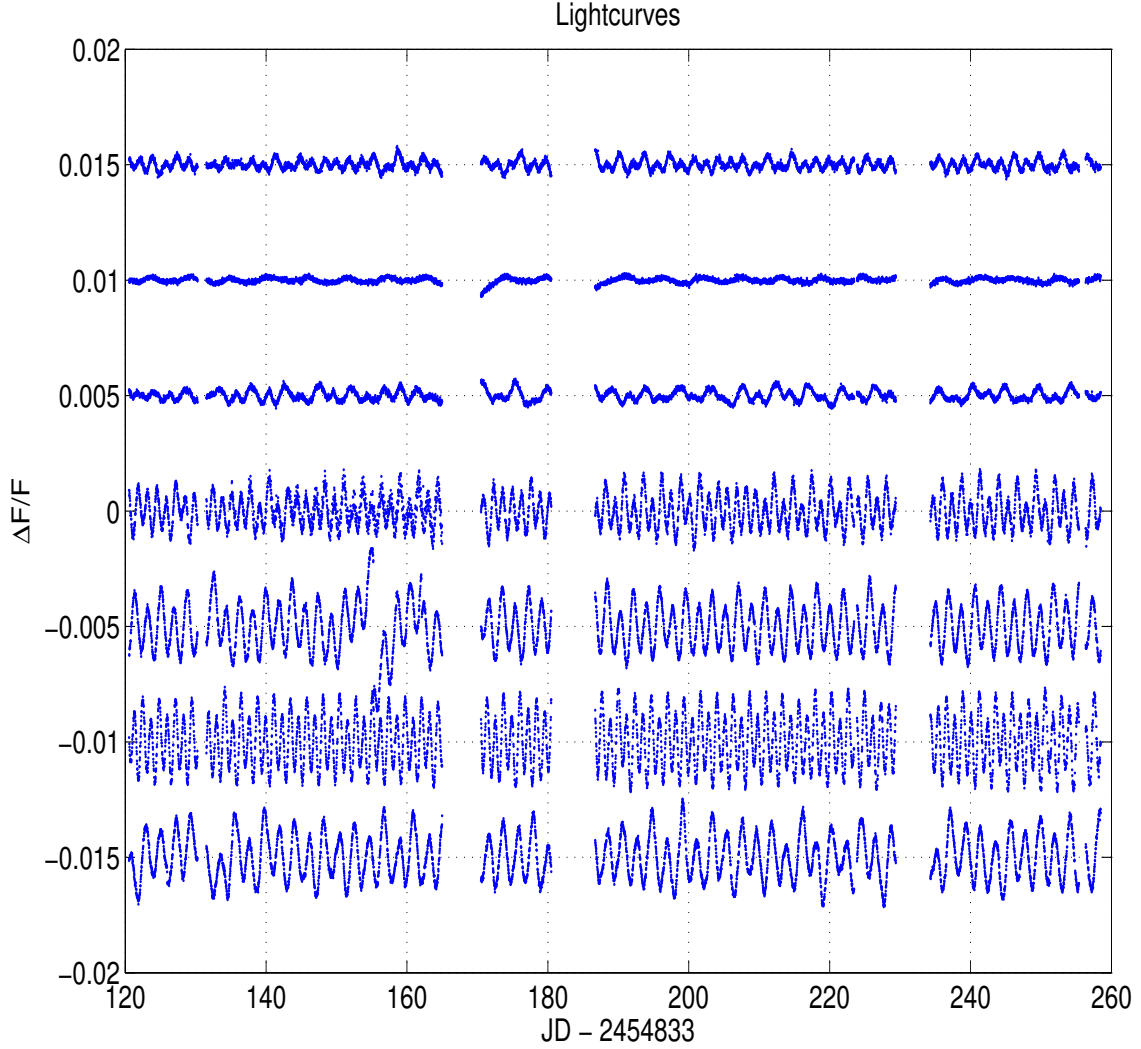


Fig. 1.— The light curves of the seven detections, after outlier removal and long-term detrending. Top to bottom: K10848064, K08016222 , K09512641, K07254760, K05263749, K04577324, K06370196. For clarity, each light curve was shifted by 5000 ppm relative to the previous one. The periodic modulation can be seen in all seven light curves. The light curves show several discontinuities: end of Q0 at day 131, end of Q1 around day 166, Q2 first safe mode event at day 183, and Q2 second safe mode event at day 232. In addition there is a single discontinuity at day 155 of the K05263749 light curve.

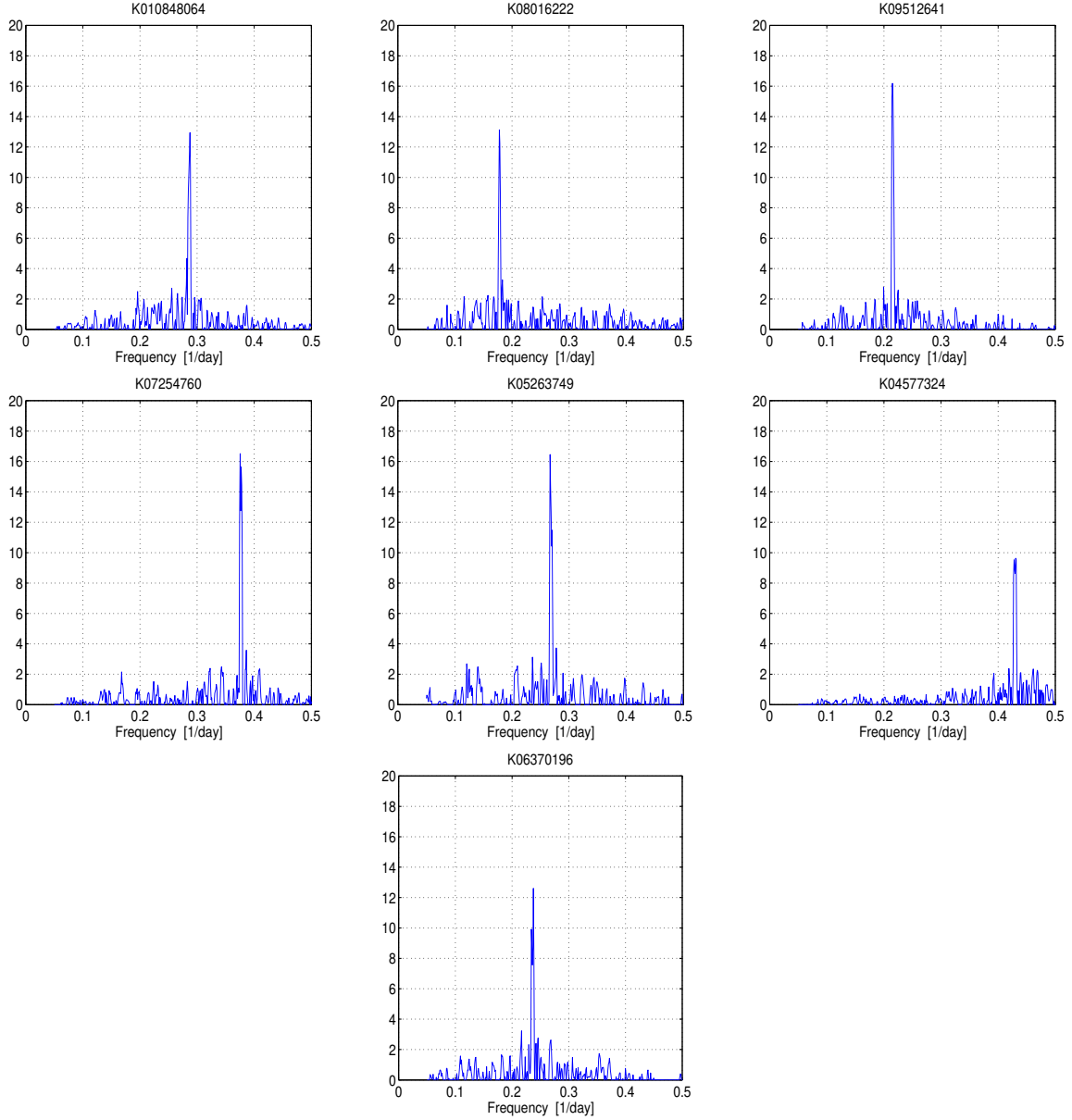


Fig. 2.— The BEER periodograms of the seven candidates. The peak frequency corresponds to the suspected orbital period. The periodograms were calculated for the period range of 0.5–20 days. For clarity, only the period range of 2–20 days is plotted, since no significant peak was found for periods smaller than 2 days in any of the periodograms. The periodograms are normalized so that the r.m.s. of the 100 noise points on two sides of the peak (50 on each side) is set to one.

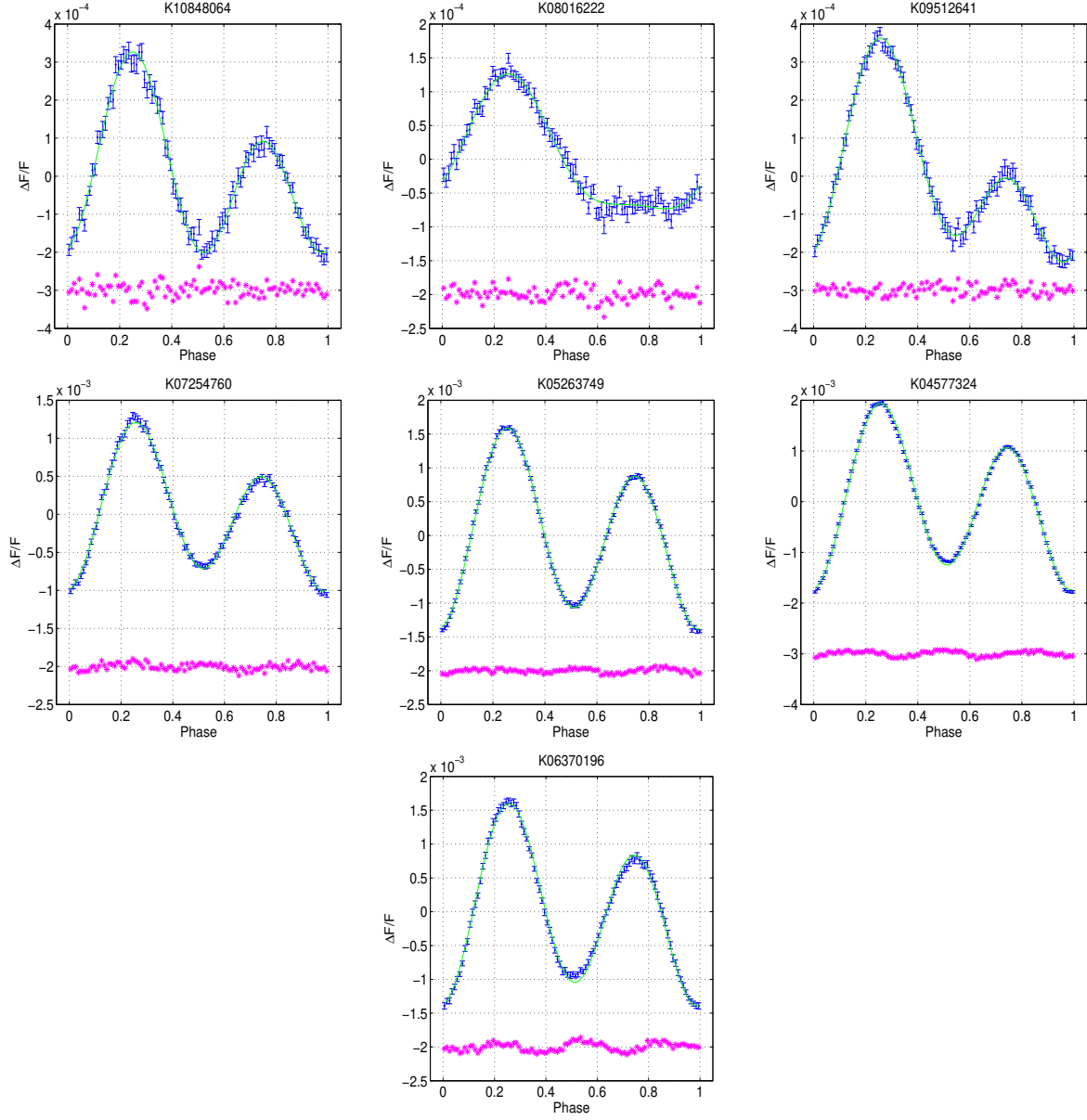


Fig. 3.— Folded cleaned light curves, binned into 100 bins, of the seven candidates. Phase zero is when the presumed companion is closest to the observer, while phase 0.5 is when the primary is closest to the observer. The errors of each bin represent 1σ estimate of the bin average value. The line presents the BEER model. The model residuals are plotted at the bottom of each figure.

3. Radial velocity observations

The RV observations were performed between 25 September 2010 and 15 June 2011 with the Tillinghast Reflector Echelle Spectrograph (TRES; Fűrész (2008)) mounted on the 1.5-m Tillinghast Reflector at the Fred Lawrence Whipple Observatory operated by the Smithsonian Astrophysical Observatory (SAO) on Mount Hopkins in Southern Arizona, using the medium fiber at a spectral resolution of 44,000, covering a spectral range from 385 to 910 nm. Exposures of a Thorium-Argon hollow-cathode lamp immediately before and after each exposure were used for wavelength calibration. The spectra were extracted and rectified to intensity vs. wavelength using standard procedures developed by Lars Buchhave (Buchhave et al. 2010).

To derive precise relative radial velocities, we performed a cross-correlation between each observed spectrum and a template spectrum constructed by shifting and co-adding all the observed spectra. In addition to the template constructed by shifting and co-adding all the observed spectra, we also tried using the strongest individual exposure of each object as the observed template. The two approaches gave essentially indistinguishable results, with slightly better residuals from the orbital fits for the shifted and co-added template. We also derived absolute velocities using the library of synthetic templates and found the same orbits, although with somewhat larger residuals.

We did not include spectral orders that were significantly contaminated by telluric lines from the Earth’s atmosphere, nor did we include the bluest orders with the lowest signal-to-noise ratio and a few red orders with known problems. The error of each relative velocity was estimated using the standard deviation of the velocities from the 21 individual orders, but the velocities themselves were derived by first co-adding the correlation functions from the 21 orders, to get a natural weighting of the contribution from each order.

Using the shifted and co-added template can distort the cross-correlation peak because

the noise in each spectrum correlates with the same noise that is still present in the averaged template, and therefore can lead to underestimated uncertainties of the velocities. To correct this effect we later inflated the uncertainties of the orbital elements (see χ_{red}^2 discussion below).

We used a library of synthetic spectra, calculated by John Laird for a grid of Kurucz model atmospheres, using a line list developed by Jon Morse (Carney et al. 1987; Latham et al. 2002), to estimate values for the effective temperature, surface gravity, metallicity, and rotational velocity of the seven primaries. This was done by cross-correlating each coadded observed template spectrum against a grid of synthetic templates surrounding the one that gave the best correlation. Our library of synthetic spectra has a spacing of 250 K in effective temperature, T_{eff} ; 0.5 in log surface gravity, $\log g$; 0.5 in the log of the metallicity compared to the sun, $[\text{m}/\text{H}]$; and has a progressive spacing for rotational velocity, v_{rot} . Because the grid is coarse, we used the correlation peak heights to interpolate between grid points, arriving at a more precise classification. Three TRES spectral orders overlap with the synthetic spectra, so we performed this cross-correlation and interpolation in each order. The mean values, weighted by the cross-correlation peak height in each order, and RMS errors are reported in Table 2. Note that because of the degeneracies between T_{eff} , $\log g$, and $[\text{m}/\text{H}]$ in the stellar spectra, correlated systematic errors may dominate. For this reason, and based on our experience in other surveys we have inflated the errors by adding 100 K in T_{eff} and 0.1 dex in $\log g$ and $[\text{m}/\text{H}]$ in quadrature to the formal order-to-order RMS errors.

The relative velocities were adjusted by a constant offset to a system of absolute velocities using observations of the nearby IAU Radial Velocity Standard Star HD 182488, whose absolute velocity was assumed to be $-21.508 \text{ km s}^{-1}$. This adjustment utilized our library of synthetic templates, from which we picked the synthetic template that gave

the best match to the observations of each star in the spectral order centered on the Mg b feature near 518 nm. This approach should avoid the problem of possible template mis-match between the various target stars and HD 182488. The uncertainty in the zero point of our absolute velocities is probably limited by the uncertainty in the absolute velocity of HD 182488, which could be as large as 100 m s^{-1} . Table 3 lists the radial-velocity measurements and their uncertainties.

For all seven candidates discussed here the first RV measurements showed clear variability. We therefore obtained enough RVs to allow orbital solutions completely independent of the BEER analysis. To determine the orbital elements of each target, *independent of the BEER results*, we ran a Markov chain Monte Carlo (MCMC) analysis of the radial velocities. We adopted values for the epoch (T), period (P), systemic velocity (γ), orbital semi-amplitude (K), eccentricity (e), and argument of periaapse (ω) corresponding to the median values of the posterior distributions. The errors listed in the tables are those corresponding to the 16th and 84th percentiles of the posterior distributions. The reported error on γ , however, includes contributions both from the formal error from the MCMC posterior and from the uncertainty in the TRES absolute zero point offset.

When the orbit is circular, the epoch reported is T_{max} , the time of maximum velocity, and when the orbit is eccentric, we report T_{peri} , the time of periastron passage. In six of

Table 2. Spectra derived stellar properties of the seven binaries

	K10848064	K08016222	K09512641	K07254760	K05263749	K04577324	K06370196
T_{eff} [K]	6209 ± 131	5919 ± 128	6348 ± 214	6377 ± 133	6328 ± 119	6515 ± 145	6213 ± 168
$\log g$ [dex]	3.68 ± 0.16	4.29 ± 0.14	4.04 ± 0.23	4.04 ± 0.23	3.54 ± 0.14	3.71 ± 0.14	3.91 ± 0.13
[m/H] [dex]	-0.24 ± 0.11	-0.14 ± 0.11	-0.37 ± 0.15	-0.04 ± 0.11	-0.21 ± 0.10	-0.08 ± 0.11	-0.26 ± 0.16
$v \sin i$ [km s ⁻¹]	14.26 ± 0.45	3.37 ± 0.24	9.47 ± 0.24	14.96 ± 0.52	21.50 ± 0.16	28.90 ± 0.36	20.93 ± 0.45

Table 3: Radial velocities of the seven binaries

Time [HJD–2455000]	RV [m s ^{−1}]	σ [m s ^{−1}]	Time [HJD–2455000]	RV [m s ^{−1}]	σ [m s ^{−1}]
K10848064:			K07254760:		
464.710256	-8835	119	694.814729	37083	39
469.624378	-17974	76	695.834208	-11894	46
488.634305	-16743	77	697.807122	15727	61
489.574441	-6552	123	699.779976	46148	83
490.617670	-17742	83	702.796583	36412	47
498.599389	-23508	57	703.815335	-11560	54
513.639601	-9108	170	704.799619	39179	51
692.888788	-13130	124	705.802918	14063	89
722.832949	-14423	43	K05263749:		
723.863233	-7328	56	694.829973	20947	69
724.857438	-21205	28	696.825053	13787	141
K08016222:			697.826976	45095	68
465.787007	-31819	63	699.974074	-12159	61
466.613973	-37012	39	701.980887	34841	87
467.723417	-33482	96	705.958593	23622	73
469.613641	-18312	42	722.851562	10492	63
485.603398	-23367	37	723.875349	45267	46
490.579108	-29588	63	724.846275	10122	75
498.591317	-22720	47	K04577324:		
722.843084	-21815	86	695.982214	-22723	166
K09512641:			697.845760	8912	99
658.935318	6324	22	703.971684	38803	87
669.855208	33915	29	722.871612	46652	99
693.803705	34608	67	723.895443	-22140	103
694.822698	16733	54	724.869757	34694	124
696.815346	17503	50	726.867639	5528	96
697.816773	34761	48	727.847462	33003	91
698.934501	27404	39	K06370196:		
701.814582	24838	40	694.852291	20398	58
702.805990	36143	39	697.835776	-13709	144
703.826109	22562	59	702.968624	22603	41
704.813460	6060	65	722.861284	-35084	114
705.813161	11855	43	723.884266	17354	76
			724.826295	8740	72
			726.857187	-47080	95
			727.797595	4696	132

seven cases, either the orbital phase coverage was not sufficient to adequately constrain the eccentricity or e was statistically indistinguishable from zero. In these cases, we fixed $e = 0$ and reran the MCMC chains, adopting T_{\max} , P , γ , and K from this solution. In one case, K08016222, the orbital phase coverage is good and e is significantly non-zero.

Figure 4 shows the RV follow-up measurements for each of the seven binaries, folded

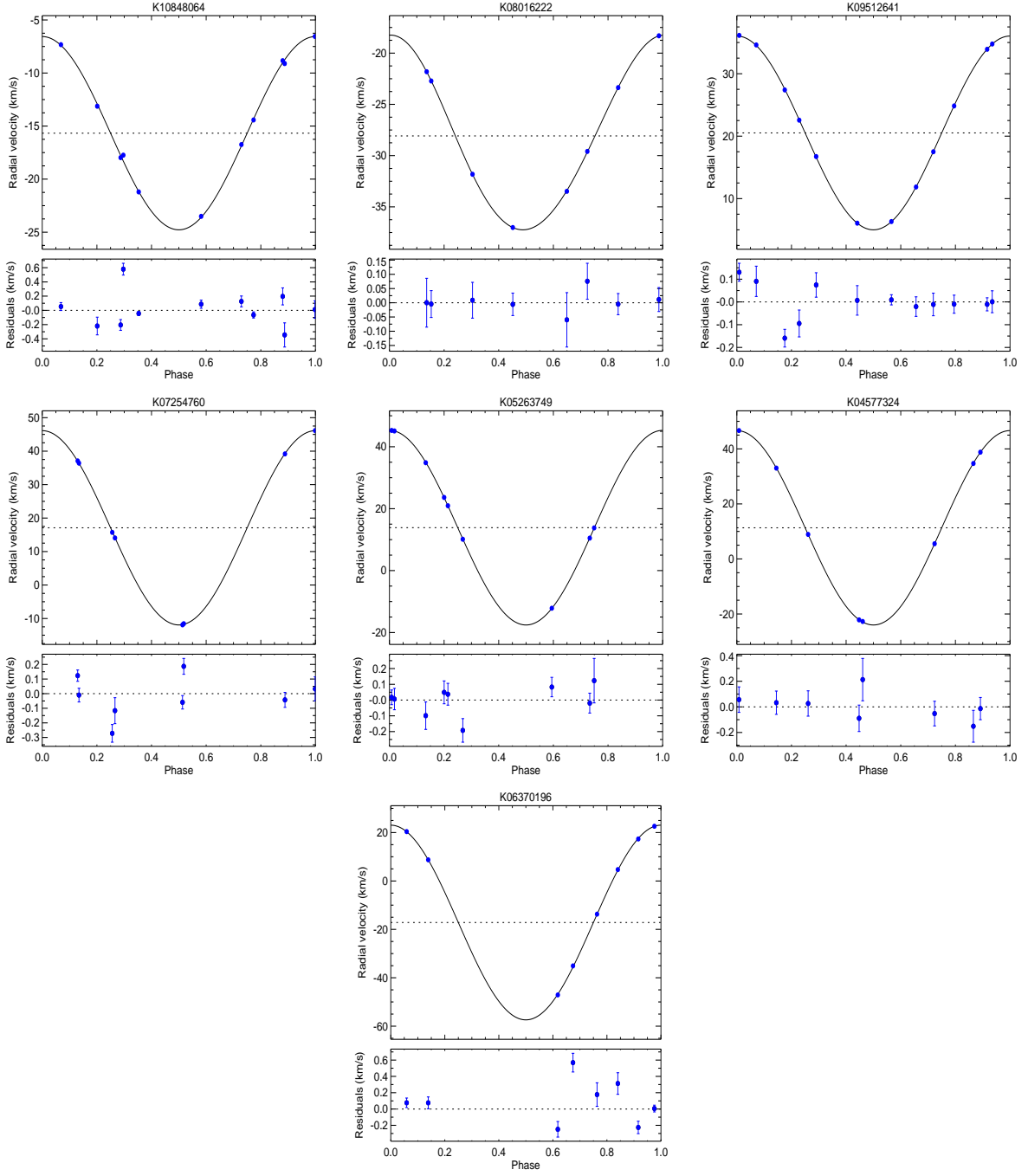


Fig. 4.— The RV measurements of the seven stars, folded at the derived orbital period. The line presents the orbital RV model. The residuals are plotted at the bottom of each figure. Note the different scale of the upper and lower panel of each star. The error bars are too small to be seen in the upper panels.

with the period found, and Table 4 lists the derived orbital elements. The table also lists χ_{red}^2 , the reduced χ^2 of the model, and the time span of the observations. For two binaries the derived χ_{red}^2 value is close to unity, as expected, but for the others its value is relatively large. This could indicate either that for those binaries our radial-velocity uncertainties are underestimated, or that our radial-velocity model is too simple, due to some stellar noise, for example. In order to get more realistic uncertainties for the model elements, we inflated the parameter uncertainties of each target by its $\sqrt{\chi_{red}^2}$, which is equivalent to inflating the RV errors of that star by the same factor. The resulting orbital model elements uncertainties are listed in Table 4.

4. Results

Table 5 lists for each of the seven newly discovered binaries the period derived from the photometry, the calculated α_{beam} , and the expected RV semi-amplitude, K_{beam} , derived from α_{beam} and the photometric beaming amplitude. The α_{beam} factor includes one component that originates from the fact that the stellar spectrum is Doppler shifted relative to the observed band. To estimate this factor for each of the seven detected binaries we numerically shifted spectra from the library of Castelli & Kurucz (2004) models that were close to the estimated temperature, metallicity and gravity of each of the seven stars. The values adopted were derived by interpolation of the α_{beam} values between the available models of the library. The α_{beam} uncertainties were estimated by calculating the interpolated α_{beam} values within the T_{eff} , $\log g$ and $[m/H]$ error ranges. The error on the expected K_{beam} was estimated by combining the photometric beaming amplitude error and the α_{beam} error. The table then reports the number of RV measurements, their derived RV period and semi-amplitude, and the minimal secondary mass, up to $\sin i$. For all cases we *independently* derived the period of the RV modulation, and found it to be consistent

Table 4. Orbital model elements of the seven binaries

	K10848064	K08016222	K09512641	K07254760	K05263749	K04577324	K06370196
$T_{\max} - 2455000$ [HJD]	465.1289 ± 0.0060	464.6288 ^a ± 0.0029	642.3690 ± 0.0052	702.4395 ± 0.0126	466.7071 ± 0.0124	466.7005 ± 0.0079	698.8374 ± 0.0035
P [days]	3.49318 ± 0.00099	5.60864 ± 0.00017	4.64588 ± 0.00044	2.65642 ± 0.00068	3.72665 ± 0.00019	2.328663 ± 0.000070	4.23371 ± 0.00067
γ [km s ⁻¹]	-15.670 ± 0.219	-28.078 ± 0.048	20.518 ± 0.110	17.092 ± 0.177	13.862 ± 0.060	11.325 ± 0.119	-17.168 ± 0.454
K [km s ⁻¹]	9.107 ± 0.073	9.495 ± 0.018	15.519 ± 0.023	29.024 ± 0.061	31.428 ± 0.040	35.316 ± 0.043	40.222 ± 0.131
e	0 (fixed)	0.0439 ± 0.0022	0 (fixed)	0 (fixed)	0 (fixed)	0 (fixed)	0 (fixed)
ω [deg]		36.2 ± 2.6					
χ_{red}^2	11.0	1.0	4.3	11.6	2.6	1.2	12.6
span [days]	260.1	257.1	46.9	11.0	30.0	31.9	32.9

^afor K08016222 the T_{\max} value is the time of periastron passage

with the photometric period, indicating that the orbital period was reliably derived by the BEER algorithm, solely from the photometric data.

In six of the binaries the eccentricity was too small to be derived significantly, so we assumed circular orbits. Because these are short-period stellar binaries, the expected circularization timescale is short, so finding in most cases that $e = 0$ is consistent with our expectations. For K08016222 we find $e = 0.0439 \pm 0.0022$. Interestingly, this is the binary with the longest period, so its lifetime might have been too short to achieve circularization (Mathieu & Mazeh 1988).

Out of the seven binaries, the measured RV amplitudes of five cases were consistent with those predicted by the photometric analysis. For the other two stars, K08016222 and K06370196, the predicted amplitudes were 24% smaller than the observed ones. This could be due to underestimation of the photometric amplitude. Another possible explanation may be an inaccurate translation of the photometric amplitude to the expected RV amplitude, which depends on the assumed stellar spectral type. We need more confirmed binaries to understand this effect.

5. Discussion

The RV observations presented here demonstrate the ability of the BEER algorithm to discover short-period binaries with minimum secondaries mass in the range of $0.07\text{--}0.4 M_{\odot}$ in the publicly available *Kepler* data.

The original goal of the *Kepler* and *CoRoT* missions was to search for transiting planets. Such projects are limited to planets with orbital inclinations close to 90° . The serendipitous discoveries of eclipsing binaries in the *Kepler* photometry (Prša et al. 2011) are suffering from the same limitation. The BEER algorithm, on the other hand, is

Table 5. Derived photometric RV period and semi-amplitude together with RV observations period and semi-amplitude for each of the seven binaries

	K10848064	K08016222	K09512641	K07254760	K05263749	K04577324	K06370196
Photometry results:							
Period [days]	3.49 ± 0.01	5.60 ± 0.02	4.65 ± 0.02	2.66 ± 0.01	3.73 ± 0.01	2.33 ± 0.01	4.23 ± 0.01
α_{beam}	0.944 ± 0.025	1.012 ± 0.023	0.912 ± 0.036	0.921 ± 0.024	0.921 ± 0.022	0.887 ± 0.025	0.936 ± 0.030
K_{beam} [km s ⁻¹]	9.37 ± 0.34	7.19 ± 0.22	15.21 ± 0.72	28.97 ± 0.89	29.14 ± 0.81	36.86 ± 1.10	30.61 ± 1.12
RV results:							
N_{obs}	11	8	12	8	9	8	8
Period [days]	3.49318 ± 0.00099	5.60864 ± 0.00017	4.64588 ± 0.00044	2.65642 ± 0.00068	3.72665 ± 0.00019	2.328663 ± 0.000070	4.23371 ± 0.00067
K_{RV} [km s ⁻¹]	9.107 ± 0.073	9.495 ± 0.018	15.519 ± 0.023	29.024 ± 0.061	31.428 ± 0.040	35.316 ± 0.043	40.223 ± 0.131
Minimum secondary mass [M_{Jup}]	76 ± 5	90 ± 6	147 ± 10	222 ± 15	279 ± 19	253 ± 17	376 ± 25

searching for *non-transiting* companions, and therefore can detect many more systems with much lower inclination angles. Searching with BEER is effectively equivalent to performing an RV survey that is not limited to nearly face-on inclinations. Applying the BEER algorithm to the hundreds of thousands of already available light curves of *Kepler* and CoRoT is like performing an RV survey of a huge sample that is composed of these stars.

Therefore, we expect BEER to discover many hundreds of new binaries with short periods. Furthermore, whereas in RV studies the actual mass of the companion depends on the unknown inclination angle, detecting *both* the ellipsoidal and the beaming effects will enable BEER to derive, or at least estimate, the mass of the small companion in certain cases. As pointed out by Faigler & Mazeh (2011), this can become possible because the two effects have different dependencies on the orbital inclination, and therefore the derived ratio of the amplitudes of the two effects can, *in principle*, remove the degeneracy between the secondary mass and the inclination.

Obviously, at this stage of the BEER search, detecting a candidate is not enough — the candidates have to be confirmed by follow-up RV observations. However, when we accumulate enough observations we will be able to estimate the false alarm probability, which might be a function of the amplitude of the photometric modulation and the stellar mass, radius and temperature. Therefore, we will be able to derive the statistical features of the short-period binaries without confirming each detection with RV observations.

The seven cases presented here were based on the Kepler Q0–Q2 data. Faigler & Mazeh (2011) suggested that once the full *Kepler* dataset is available, we should be able to detect brown-dwarf secondaries and even massive planets. Moreover, the other stellar modulations that contribute now to the false alarm frequency are not expected to be so stable on time scales of years, whereas the three BEER effects are strictly periodic and stable. Therefore, we expect the false alarm frequency to decrease when we have access to longer data sets.

The unprecedentedly large sample size and data quality, together with a knowledge of the false alarm probability, could serve as a tool to study accurately the frequency of low-mass secondaries in short-period binaries on the high- and low-mass ends of the brown-dwarf desert (Raghavan et al. 2010; Udry 2010; Sahlmann et al. 2010).

We are indebted to Shay Zucker and Ehud Nakar for helpful discussions. We thank the anonymous referee for highly illuminating comments and suggestions.

We feel deeply indebted to the team of the Kepler mission, that enabled us to search and analyze their unprecedentedly accurate photometric data.

All the photometric data presented in this paper were obtained from the Multimission Archive at the Space Telescope Science Institute (MAST). STScI is operated by the Association of Universities for Research in Astronomy, Inc., under NASA contract NAS5-26555. Support for MAST for non-HST data is provided by the NASA Office of Space Science via grant NNX09AF08G and by other grants and contracts.

We thank the Kepler mission for partial support of the spectroscopic observations under NASA Cooperative Agreement NNX11AB99A with the Smithsonian Astrophysical Observatory, DWL PI.

This research was supported by the ISRAEL SCIENCE FOUNDATION (grant No. 655/07).

Facilities: FLWO:1.5m (TRES)

REFERENCES

- Aigrain, S., Favata, F., & Gilmore, G. 2004, *A&A*, 414, 1139
- Auvergne, M., et al. 2009, *A&A*, 506, 411
- Baglin, A., et al. 2006, 36th COSPAR Scientific Assembly, 36, 3749
- Bloemen, S., et al. 2011, *MNRAS*, 410, 1787
- Borucki, W. J., et al. 2010, *Science*, 327, 977
- Brown, T. M., Latham, D. W., Everett, M. E., & Esquerdo, G. A. 2011, arXiv:1102.0342
- Buchhave, L. A., et al. 2010, *ApJ*, 720, 1118
- Carney, B. W., Laird, J. B., Latham, D. W., & Kurucz, R. L. 1987, *AJ*, 93, 116
- Carter, J. A., Rappaport, S., & Fabrycky, D. 2011, *ApJ*, 728, 139
- Castelli, F., & Kurucz, R. L. 2004, arXiv:astro-ph/0405087
- Faigler, S., & Mazeh, T. 2011, *MNRAS*, 1106
- For, B.-Q., et al. 2010, *ApJ*, 708, 253
- Fűrész, G., Ph.D. thesis, University of Szeged, Hungary
- Harrison, T. E., Howell, S. B., Huber, M. E., Osborne, H. L., Holtzman, J. A., Cash, J. L.,
& Gelino, D. M. 2003, *AJ*, 125, 2609
- Kipping, D. M., & Spiegel, D. S. 2011, arXiv:1108.2297
- Koch, D. G., et al. 2010, *ApJ*, 713, L79
- Latham, D. W., Stefanik, R. P., Torres, G., Davis, R. J., Mazeh, T., Carney, B. W., Laird,
J. B., & Morse, J. A. 2002, *AJ*, 124, 1144

- Loeb, A., & Gaudi, B. S. 2003, *ApJ*, 588, L117
- Mathieu, R. D., & Mazeh, T. 1988, *ApJ*, 326, 256
- Maxted, P. F. L., Marsh, T. R., Heber, U., Morales-Rueda, L., North, R. C., & Lawson, W. A. 2002, *MNRAS*, 333, 231
- Mazeh, T. 2008, *EAS Publications Series*, 29, 1
- Mazeh, T., & Faigler, S. 2010, *A&A*, 521, L59
- Morris, S. L. 1985, *ApJ*, 295, 143
- Prša, A., et al. 2011, *AJ*, 141, 83
- Raghavan, D., et al. 2010, *ApJS*, 190, 1
- Reed, M. D., et al. 2010, *Ap&SS*, 329, 83
- Rouan, D., Baglin, A., Copet, E., Schneider, J., Barge, P., Deleuil, M., Vuillemin, A., & Léger, A. 1998, *Earth Moon and Planets*, 81, 79
- Rowe, J. F., et al. 2010, *ApJ*, 713, L150
- Rybicki, G. B., & Lightman, A. P. 1979, *Radiative Processes in Astrophysics* (New York: Wiley)
- Sahlmann, J., Segransan, D., Queloz, D., & Udry, S. 2010, *arXiv:1012.1319*
- Udry, S. 2010, *In the Spirit of Lyot 2010*,
- Wilson, R. E. 1990, *ApJ*, 356, 613
- van Kerkwijk, M. H., Rappaport, S. A., Breton, R. P., Justham, S., Podsiadlowski, P., & Han, Z. 2010, *ApJ*, 715, 51

Vaz, L. P. R. 1985, *Ap&SS*, 113, 349

Zucker, S., Mazeh, T., & Alexander, T. 2007, *ApJ*, 670, 1326